

2010

Energy Barrier, Charge Carrier Balance, and Performance Improvement in Organic Light-Emitting Diodes


Pavel Anzenbacher Jr.
Bowling Green State University, pavel@bgsu.edu

Amare Benor

Shin-ya Takizawa

C. Pérez-Bolivar

Follow this and additional works at: https://scholarworks.bgsu.edu/chem_pub

 Part of the [Chemistry Commons](#)

Repository Citation

Anzenbacher, Pavel Jr.; Benor, Amare; Takizawa, Shin-ya; and Pérez-Bolivar, C., "Energy Barrier, Charge Carrier Balance, and Performance Improvement in Organic Light-Emitting Diodes" (2010). *Chemistry Faculty Publications*. 22.
https://scholarworks.bgsu.edu/chem_pub/22

This Article is brought to you for free and open access by the Chemistry at ScholarWorks@BGSU. It has been accepted for inclusion in Chemistry Faculty Publications by an authorized administrator of ScholarWorks@BGSU.

Energy barrier, charge carrier balance, and performance improvement in organic light-emitting diodes

Amare Benor, Shin-ya Takizawa, C. Pérez-Bolivar, and Pavel Anzenbacher, Jr.^{a)}

Center for Photochemical Sciences, Bowling Green State University, Bowling Green, Ohio 43403, USA

(Received 30 March 2010; accepted 19 May 2010; published online 18 June 2010)

The charge injection properties of poly(3,4-ethylenedioxythiophene):polystyrene sulfonate anodes are crucial for performance of organic photovoltaics and organic light-emitting diodes (OLEDs). A simple method for tuning hole injection efficiency using UV-ozone is shown to change anode work-function and optimized carriers balance in the devices and improved efficiency in OLEDs. The optimum time of treatment and work-function differs with device architecture. © 2010 American Institute of Physics. [doi:10.1063/1.3452344]

High performance organic light-emitting diodes (OLEDs),¹ photovoltaics,² and transistors³ are desired for displays, including large-area devices and in solid state lighting.⁴ Doping of semiconductor,^{5,6} stacked emissive layers,⁵ and additional layers to control charge injection and transport⁶ are the methods used to improve device efficiency. The charge carrier injection optimization is a crucial factor for OLED. When the surface states or dipole effect/barrier (Δ) at the interface is not considered, the energy barrier (ϕ_B) for hole injection (HI) is $\phi_B^h = I - \Phi_{\text{anode}}$, where Φ is electrode work-function, and I is ionization energy of the organic layer.⁷ However, the presence of surface state or dipole barrier Δ has an effect in electrode-organics interfaces and the actual energy barrier may change significantly.^{8,9} Based on the magnitude of the actual energy barriers, an OLED can be of either injection limited, space charge, or bulk limited for a barrier less than 0.25–0.3 eV.⁹

Often, the barriers are higher and the OLEDs are injection limited. Hence, the charge injection efficiency determines charge balance and efficiency, and can be used for OLED optimization. Despite the fact that the balanced charge injection is important in OLEDs fabrication, only few studies explored this issue.^{10–13} Typically, methods used to control HI is variation in thickness of the injection material such as copper phthalocyanine (CuPc),^{10,14} which does not allow for tuning of the work function of the hole injecting material (HIM). Due to its potential for low-cost device fabrication, poly(3,4-ethylenedioxythiophene):polystyrene sulfonate (PEDOT:PSS) emerged as one of the most important HIM. Therefore, we developed a method to control HI compatible with large area processing focused on shifting the work function of a PEDOT:PSS hole-injection layer (HIL) via UV-ozone treatment.¹⁵ As a result, up to threefold (e.g., from 3.5% to 10.5%) improvement in external quantum efficiency (EQE) OLEDs was realized.¹⁵ This earlier study focused solely on the optical characteristics of the OLEDs. Following our report, Helander *et al.*⁹ utilized hole-only devices (HOD) to provide an insight into the barrier injection in the UV-ozone treated PEDOT:PSS anodes. While this study extended our understanding of the underlying physics, given the limitation of the HODs, it did not address the impact on electroluminescence and efficiency. Here, we provide

a detailed summary of the physics governing the electrical properties of the OLEDs, charge injection efficiency, the difference in time of exposure for maximum efficiency of different OLEDs, and the effect on the optical characteristics or EQE. Finally, to illustrate the potential of the method, we provide a comparison between phosphorescent and fluorescent OLEDs.

First, we studied the injection efficiency from the indium tin oxide (ITO)-PEDOT:PSS anode to a hole transport layer (HTL) of 4,4'-bis[*N*-(1-naphthyl)-*N*-phenyl amino]biphenyl (α -NPD) as it depends on the PEDOT:PSS UV-ozone exposure time (0–8 min) in a HOD. At and beyond 10 min of UV-ozone treatment, the PEDOT:PSS anode displayed etching and pinholes that lowered the reproducibility of the results. The injection efficiency (η_{inj}) was related to the UV-ozone induced change in the injection barrier, work-function, and the overall performance in OLEDs. The time of treatment for the maximum efficiency related to the injection barrier was studied using different device configurations utilizing phosphorescent and fluorescent OLEDs. We used four green emitting OLEDs with following configurations. *Device I*: ITO/PEDOT:PSS (30 nm)/ α -NPD (40 nm)/1,3,5-tris(*N*-phenylbenzimidazol-2-yl)benzene (TPBI) doped with 6% iridium(III) bis(2-phenylpyridinato-*N*, *C*^{2'}) acetylacetonate [Ir(ppy)₂(acac)] (50 nm)/CsF (1 nm)/Al (100 nm); *Device II*: ITO/PEDOT:PSS (30 nm)/ α -NPD (30 nm)/4,4',4''-tris(*N*-carbazolyl)triphenylamine (TCTA) (10 nm)/TPBI:6% Ir(ppy)₂(acac) (50 nm)/CsF (1 nm)/Al (100 nm); *Device III*: ITO/PEDOT:PSS (30 nm)/ α -NPD (40 nm)/tris(8-quinolinolato) aluminum (Alq₃) doped with 1% 2,3,6,7-tetrahydro-1,1,7,7-tetramethyl-1H,5H,11H-10-(2-benzothiazolyl)quinolizino-(9,9a,1gh)coumarin (C545T) (40 nm)/Alq₃ (30 nm)/CsF (1 nm)/Al (100 nm); and *Device IV*: ITO/PEDOT:PSS (30 nm)/ α -NPD (40 nm)/Alq₃ (30 nm)/CsF (1 nm)/Al (100 nm). Devices I and II are phosphorescent OLEDs with the same layers except that device II shows a more optimized charge balance as it comprises an electron/exciton blocking layer of TCTA. Devices III and IV are fluorescent OLEDs, whereas device III utilizes emissive layer consisting of electron transport material (Alq₃) doped with C545T while the Alq₃ layer in the device IV was left undoped serving both as an electron-transporting and an emitter. The device fabrication was performed by spin-coating of the PEDOT:PSS (Clevios PVP Al 4083) followed by evaporation of the remaining layers.¹⁶ In all devices, the

^{a)} Author to whom correspondence should be addressed. Electronic mail: pavel@bgsu.edu.

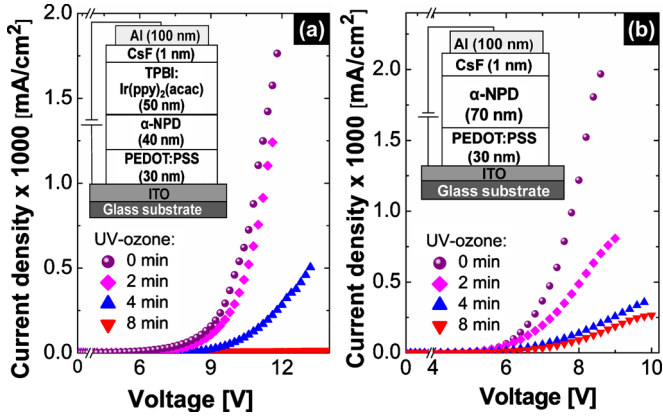


FIG. 1. (Color online) Current density-voltage (J vs V) curves at 0, 2, 4, and 8 min of UV-ozone treatment of PEDOT:PSS in Device I (a) and HOD (b).

PEDOT:PSS layer was treated by UV-ozone (PSD-UV, Novascan) for 2, 4, and 8 min and compared to the control device with untreated PEDOT:PSS HIL.

Figure 1(a) presents J - V curves using a different time of UV-ozone exposure of the HIL. We found that the current density (J) decreases as the UV-ozone exposure time increases from 0 to 8 min. Thus, the charge injection and the corresponding η_{inj} from the HIL to the HTL is affected by the UV-ozone exposure. To calculate the charge η_{inj} from ITO to a HTL through the PEDOT:PSS injection layer, two parameters are required:¹⁰ (I) current density of a trap-free space charge-layer (TFSCl) limited current density (J_{TFSCl}), and (II) measured current density, J_{MEAS} , of the sample. Here, we used a HOD of the following architecture: ITO/PEDOT:PSS (30 nm)/ α -NPD (70 nm)/CsF (1 nm)/Al (100 nm) [Fig. 1(b)]. The TFSCl layer current density, J_{TFSCl} , is given by Child's law,^{17,18}

$$J_{TFSCl} = (9/8)\epsilon\epsilon_0\mu V^2/d^3, \quad (1)$$

where ϵ and ϵ_0 are the relative dielectric constant of the organic layer and the permittivity of the free space, respectively, and d is the device thickness. ϵ is assumed as 3.0 and the ϵ_0 is 8.85×10^{-14} C/V cm.¹⁹ From the time of flight measurements, the hole mobility $\mu \sim 3.25 \times 10^{-4}$ cm²/V s.²⁰ Here, we consider a constant mobility as it is only weakly dependent on electric field.²⁰ The η_{inj} at a given voltage is $\eta_{inj} = J_{MEAS}/J_{TFSCl}$. Because η_{inj} changes as the voltage varies, we use an average of the η_{inj} from the fitted curves of J_{MEAS} and J_{TFSCl} . The J_{MEAS} and J_{TFSCl} values were fitted by $J = aV^2 \exp(-b/V)$, where a and b are constants and V is the voltage. As a result, the average η_{inj} within the voltage range of 0.0 and v is simplified by equation:

$$\eta_{inj} = \frac{1}{v} \int_0^v \frac{J_{MEAS}(V)}{J_{TFSCl}(V)} dV. \quad (2)$$

Figure 2(a) shows the L - V curves of device I with PEDOT:PSS layer treated for 0, 2, 4, and 8 min UV-ozone, an effect that was not described previously.^{9,15} To understand this feature, two aspects were considered for the different exposure times: (I) injection efficiency of HOD, and (II) the current (I) and L at a given operating voltage (7 V) of device I. Figure 2(b) shows the calculated η_{inj} corresponding to the UV-ozone exposure time from 0 to 8 min. The η_{inj} decreases exponentially from ~ 0.425 (42.5%) at 0 min to ~ 0.020

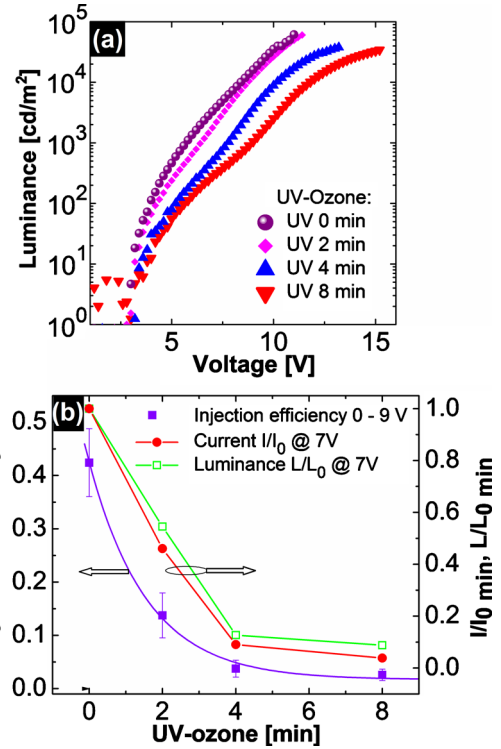


FIG. 2. (Color online) (a) Luminance-voltage (L - V) curves of Device I at different time of exposure; (b) η_{inj} of HOD from 0 to 9 V (10% error bar), and current (I)/ L (ratio at a given time vs 0 min) of Device I at 7 V as function of time of UV-ozone exposure.

(2%) at 8 min. From the exponential fit, one can see that the η_{inj} seems to be almost constant after ~ 7 or 8 min of the UV-ozone exposure, which indirectly supports our observation that there is no significant change in device performance after 8 min of exposure, i.e., the change in PEDOT:PSS work-function is saturated at 8 min. Experiments suggest that treatment beyond 8 min does not yield further changes in device performance. The η_{inj} implies that the injected current decreases exponentially as the barrier height increases linearly.¹³ The barrier height increases as the UV-ozone exposure time increases from 0 to 8 min with increments of PEDOT:PSS work function (in absolute value). The untreated PEDOT:PSS/ α -NPD with a dipole barrier of 0.25–0.30 eV corresponds to an energy barrier 0.75–0.80 eV.^{8,9} On the other hand, for 8 min UV-ozone treatment the energy barrier is ~ 0.90 eV, which corresponds to an increase of 0.15 eV compared to the untreated layer.⁹ As a result of the UV-ozone exposure, η_{inj} decreases exponentially while the injection barrier increases linearly.²¹ This trend can also be used to estimate the time required to reach the saturation of change in the energy barrier. Thus, our study shows that η_{inj} in OLEDs can be tuned by UV-ozone exposure as a result of shifting the level of the PEDOT:PSS work function and dipole barrier. The treatment can be used to optimize charge carriers density at an emissive layer by tuning the injection at one electrode, thus providing easy-to-do method to optimize OLEDs efficiency.

In Fig. 2(a), L in device I decreases with the exposure time. A similar trend is observed in other OLEDs fabricated at different time of PEDOT:PSS exposure. However, Fig. 2(b) shows that I and L ratios at various times 0–8 min at 7 V decrease with the exposure time. Thus, the decrease in L while the exposure time increases is due to the decrease in I ,

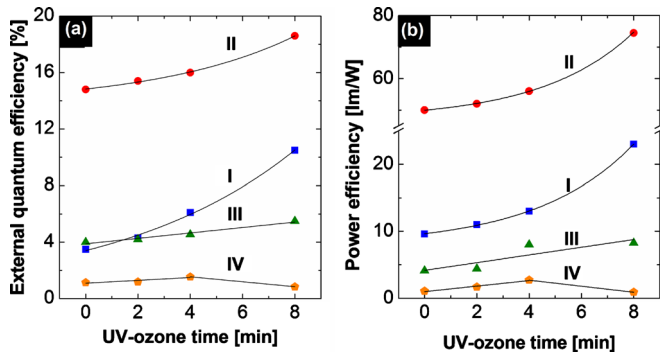


FIG. 3. (Color online) EQE (a) and PE (b) of devices I, II, III, and IV at 0, 2, 4, and 8 min of UV-ozone exposure. The fits for the phosphorescent OLEDs (I and II) are exponential while the fluorescent OLEDs (III and IV) are linear.

which is due to the increased hole energy barrier (ϕ_B^h) between 0 and 8 min. The main question that arises is to what extent a current supply is used for each emissive event at a given voltage. i.e., the maximum EQE of the device for each architecture and the time of the UV-ozone treatment.

Next, the efficiency was studied as a function of the UV-ozone exposure time of the HIL. The device efficiency is indirectly related to η_{inj} and is, in turn, controlled by the energy barrier. This is demonstrated by varying the exposure time from 0 to 8 min for the two fluorescent and the two phosphorescent OLEDs. The turn-on voltage for the fluorescent OLEDs was 2.5–3.5 V, and ~ 2.5 V for phosphorescent OLEDs. The trend observed for the J - V curve described in Fig. 1(a) is similar for all devices. Due to the decreased η_{inj} , J at a given voltage decreases with the exposure time but the degree of charge utilization in radiative processes is higher.

Figure 3 presents the EQE and the corresponding power efficiency (PE) of the four OLED architectures as a function of UV-ozone exposure time. The EQE was modestly increased by 0.4% (from 1.15% at 0 min to 1.55% at 4 min) for device IV up to a threefold increase for device I (from 3.5% at 0 min to 10.5% at 8 min). The corresponding PE of the devices was increased from 1.05 at 0 min to 2.7 lm/W at 4 min for device IV and from 9.6 at 0 min to 23 lm/W at 8 min for device I (Fig. 3). At the maximum EQE in device IV the η_{inj} is ~ 0.037 , which corresponds to a hole barrier of ~ 0.87 eV. In devices I–III, at the maximum EQE the η_{inj} is ~ 0.020 , which corresponds to the maximum injection barrier of about 0.90 eV (8 min of the exposure). The trend in efficiency improvement, as observed from the fits in Figs. 3(a) and 3(b) is linear for fluorescence-based devices (III and IV) and exponential for phosphorescent OLEDs (I and II). Thus, devices III and IV showed a dramatic increase in the efficiency (up to threefold) compared to the fluorescent OLEDs. This tendency is particularly obvious in the EQE of device I and device III. Without the UV-ozone treatment, device III displays EQE comparable to the phosphorescent OLED I. However, after 8 min of the UV-ozone treatment, the EQE of the phosphorescent device I is twice higher than the fluorescent device III.

The device efficiency varies with time of UV-ozone exposure, which indicates that the different η_{inj} is controlled by shifting the PEDOT:PSS anode work function and the inter-

face dipole barriers. The shift is presumed to be due to oxidation of the PEDOT:PSS.¹³ The balanced charge injection, a crucial factor in improving OLEDs efficiency, for different devices is achieved at different η_{inj} (or time of the exposure) and depends on the device configuration.

In summary, we have studied the effect of η_{inj} from the anode to the HTL with increasing time of UV-ozone exposure (from 0 to 8 min), which is related to the corresponding change in the work function of PEDOT:PSS and the interface dipole barrier. The study showed that η_{inj} decreases exponentially and tends to be constant after ~ 8 min of UV-ozone exposure showing that the change in the injection efficiency reached limit. The η_{inj} can be tuned by the exposure and is related to the OLED efficiency. The use of UV-ozone exposure treatment enhances the OLED performances by optimizing injected charge carriers. The trend in the device efficiency improvement depends on the type of device configuration. Phosphorescent OLEDs show exponential increase in EQE and PE reaching 18% and 75 lm/W, respectively. This method offers an easy-to-do method for optimizing charge carriers balance to improve OLEDs efficiency.

Financial support from AFOSR (Grant No. FA9550-05-1-0276 to P.A.), the State of Ohio (WCI-PVIC), and BGSU is gratefully acknowledged.

¹Highly Efficient OLEDs with Phosphorescent Materials, edited by H. Yersin (Wiley, Weinheim, 2009).

²Organic Photovoltaics: Materials, Device Physics, and Manufacturing Technologies, edited by C. Brabec, V. Dyakonov, and U. Scherf (Wiley, Weinheim, 2008).

³Physical and Chemical Aspects of Organic Electronics: From Fundamentals to Functioning Devices, edited by C. Wöll (Wiley, Weinheim, 2008).

⁴G. Held, Introduction to Light Emitting Diode Technology and Applications (CRC/Taylor & Francis, Boca Raton, FL, 2009).

⁵K. Walzer, B. Maennig, M. Pfeiffer, and K. Leo, Chem. Rev. (Washington, D.C.) **107**, 1233 (2007).

⁶Y. Shirota and H. Kageyama, Chem. Rev. (Washington, D.C.) **107**, 953 (2007).

⁷M. Pope and C. E. Swenberg, Electronic Processes in Organic Crystals (Clarendon, Oxford, 1982).

⁸A. Kahn, N. Koch, and W. Y. Gao, J. Polym. Sci., Part B: Polym. Phys. **41**, 2529 (2003).

⁹M. G. Helander, Z. B. Wang, M. T. Greiner, Z. W. Liu, K. Lian, and Z. H. Lu, Appl. Phys. Lett. **95**, 173302 (2009).

¹⁰E. W. Forsythe, M. A. Abkowitz, and Y. Gao, J. Phys. Chem. B **104**, 3948 (2000).

¹¹F. Li, Z. Chen, C. Liu, and Q. Gong, Chem. Phys. Lett. **412**, 331 (2005).

¹²L. Aubouy, N. Huby, L. Hirsch, A. Lee, and P. Gerbier, New J. Chem. **33**, 1290 (2009).

¹³M. Y. Chan, S. L. Lai, M. K. Fung, C. S. Lee, and S. T. Lee, J. Appl. Phys. **95**, 5397 (2004).

¹⁴L. Zou, V. Savate'ev, J. Booher, C.-H. Kim, and J. Shinar, Appl. Phys. Lett. **79**, 2282 (2001).

¹⁵A. Benor, S. Takizawa, P. Chen, C. P. Bolívar, and P. Anzenbacher, Jr., Appl. Phys. Lett. **94**, 193301 (2009).

¹⁶V. Montes, R. Pohl, J. Shinar, and P. Anzenbacher, Jr., Chem.-Eur. J. **12**, 4523 (2006).

¹⁷N. F. Mott and R. W. Gurney, Electronic Processes in Ionic Crystals (Clarendon, Oxford, 1940).

¹⁸M. A. Lampert and P. Mark, Current Injection in Solids (Academic, New York, 1970).

¹⁹T.-Y. Chu and O.-K. Song, Appl. Phys. Lett. **90**, 203512 (2007).

²⁰S. W. Tsang, S. C. Tse, K. L. Tong, and S. K. So, Org. Electron. **7**, 474 (2006).

²¹M. Petrosino, P. Vacca, R. Miscioscia, G. Nenna, C. Minarini, and A. Rubino, Proc. SPIE **6593**, 659310 (2007).